Nearly quantum-limited microwave amplification via interfering degenerate stimulated emission in a single artificial atom

npj | quantum information

Published in partnership with The University of New South Wales

Article

https://doi.org/10.1038/s41534-025-00993-3

Nearly quantum-limited microwave amplification via interfering degenerate stimulated emission in a single artificial atom

Fahad Aziz[1,2,14], Kuan-Ting Lin[3,4,14], Ping-Yi Wen[5,14], Samina[1], Yu-Chen Lin[3], Emely Weigand[6], Ching-Ping Lee[1], Yu-Ting Cheng[1], Yong Lu[7,8,9], Ching-Yeh Chen[1], Chin-Hsun Chien[1], Kai-Min Hsieh[1], Yu-Huan Huang[1], Haw-Tyng Huang[10], Hou Ian[11,12], Jeng-Chung Chen[1], Yen-Hsiang Lin[1], Anton Frisk Kockum[6], Guin-Dar Lin[3,4,13] & Io-Chun Hoi[2] ✉

Reaching the quantum limit for added noise in amplification processes is an important step toward many quantum technologies. Nearly quantum-limited traveling-wave parametric amplifiers with Josephson junction arrays have been developed and recently even become commercially available. However, the fundamental question of whether a single atom also can reach this quantum limit has not yet been answered in practice. Here, we investigate the amplification of a microwave probe signal by a superconducting artificial atom, a transmon, at the end of a semi-infinite transmission line, under a strong pump field. The end of the transmission line acts as a mirror for microwave fields. Due to the weak anharmonicity of the artificial atom, the strong pump field creates multi-photon excitations among the dressed states. Transitions between these dressed states, Rabi sidebands, give rise to either amplification or attenuation of the weak probe. We obtain a maximum power amplification of 1.402 ± 0.025, higher than in any previous experiment with a single artificial atom. We achieve near-quantum-limited added noise (0.157 ± 0.003 quanta; the quantum limit is 0.143 ± 0.006 quanta for this level of amplification), due to quantum coherence between Rabi sidebands, leading to constructive interference between emitted photons.

Stimulated emission[1], a fundamental phenomenon that is at the heart of modern laser and maser technology, plays a key role in amplifiers[2]. This process occurs when an incident photon interacts with a fully excited (population inversion) two-level atom, resulting in the emission of an additional photon, leading to a power gain G of 2, with added noise of one quantum. The quantum limit for the noise is[3]

$$\mathrm{QLN} \geq \frac{1}{2}\left|1 - \frac{1}{G}\right|, \tag{1}$$

i.e., 0.25 quanta for the gain in this example. To achieve quantum-limited added noise, this mechanism can be extended to a multi-level atom with a multi-photon pump. In such a system, it is possible to have emissions with the same energy from two different dressed-state transitions with population inversion. If these emissions do not interfere, the total emitted intensity I will be the sum of the individual intensities, i.e., $I = |\overrightarrow{E_1}|^2 + |\overrightarrow{E_2}|^2 \approx 2|E|^2$, where $E \equiv E_1 \approx E_2$ is the electric field of individual emission. With quantum interference, the maximum intensity

[1]Department of Physics, National Tsing Hua University, Hsinchu, 30013, Taiwan. [2]Department of Physics, City University of Hong Kong, Tat Chee Avenue, 999077 Kowloon, Hong Kong SAR, China. [3]Department of Physics and CQSE, National Taiwan University, 10617 Taipei, Taiwan. [4]Trapped-Ion Quantum Computing Laboratory, Hon Hai Research Institute, Taipei, 11492, Taiwan. [5]Department of Physics, National Chung Cheng University, Chiayi, 621301, Taiwan. [6]Department of Microtechnology and Nanoscience, Chalmers University of Technology, 412 96 Gothenburg, Sweden. [7]Guangzhou Institute of Technology, Xidian University, Xi'an, China. [8]Advanced Interdisciplinary Research Center, Xidian University, Xi'an, China. [9]Faculty of Integrated Circuit, Xidian University, Xi'an, China. [10]Department of Materials Science and Engineering, National Taiwan University, Taipei, 10617, Taiwan. [11]Institute of Applied Physics and Materials Engineering, University of Macau, Macau, China. [12]UMacau Zhuhai Research Institute, Zhuhai, Guangdong, China. [13]Physics Division, National Center for Theoretical Sciences, Taipei, 10617, Taiwan. [14]These authors contributed equally: Fahad Aziz, Kuan-Ting Lin, Ping-Yi Wen. ✉e-mail: iochoi@cityu.edu.hk

becomes $I = (\overrightarrow{E_1} + \overrightarrow{E_2})^2 = |\overrightarrow{E_1}|^2 + |\overrightarrow{E_2}|^2 + 2\overrightarrow{E_1} \cdot \overrightarrow{E_2} \approx 4|E|^2$ when $\overrightarrow{E_1}$ and $\overrightarrow{E_2}$ are in phase. The dot-product term represents the contribution from the interference. Thus, the emission intensity, and thus the gain, with quantum constructive interference can be twice that of emission without quantum interference. Crucially, the added noise is the same for both cases. Here, we utilize these properties to achieve nearly quantum-limited added noise in amplification with a single artificial multi-level atom.

To explore amplification by stimulated emission from atoms in a three-dimensional open space is challenging since atoms and electromagnetic fields only interact weakly there, due to spatial mode mismatch[4]. However, the interaction can be increased by confining an atom to interact with the continuum field in a one-dimensional open waveguide[5,6]; one realization of such a setup is with a single artificial atom in an open transmission line[7]. The study of numerous quantum optical effects in such setups has paved the way for the emerging field of waveguide quantum electrodynamics (QED)[8–20].

Existing amplification schemes in waveguide QED have employed various mechanisms, such as population inversion between bare states[7], population inversion between dressed states[21], and amplification without population inversion due to higher-order processes between dressed states[22]. However, none of those schemes have led to experimentally measured amplitude (power) amplification of more than 1.09 (1.19), nor noise close to the quantum limit. Here, we demonstrate a significant improvement in the amplification of the probe field using quantum coherence between the Rabi sidebands of a strongly driven superconducting artificial atom at the end of a semi-infinite transmission line; at the same time, we also achieve nearly quantum-limited noise. The mechanism, which builds on top of an essentially half-waveguide-QED system, differs from previous work[21], where the artificial atom was coupled to an open transmission line and only a two-photon pump was investigated. Due to the weak anharmonicity of the artificial atom, the strong pump field not only generates stable dressed states but also produces population inversion across them. The key difference between this work and others[7,21,22] is the degenerate stimulated emission.

We investigate the cases of two-photon, three-photon, and four-photon pumping, which result in multiple Rabi sidebands that lead to either amplification or attenuation of the weak probe. When two amplification Rabi sidebands cross, the emitted photons from one sideband interfere constructively with those from the other sideband to further enhance amplification. In addition, the one-dimensional and unidirectional output ensures perfect interference between the two amplification Rabi sidebands and eliminates the disadvantage of losing half of the stimulated emission due to the bidirectional output in a waveguide-QED system[23]. We also engineer the artificial atom to have a relaxation rate much faster than its pure dephasing rate, which further improves amplification. With all these effects combined, we obtain a maximum power amplification of $G = 1.402 \pm 0.025$, higher than any previous work with a single artificial atom[7,21,22]. At the same time, our experiment is the first in such a setup to achieve nearly quantum-limited added noise. By analyzing the spectrum of spontaneous emission, we find that the added noise in our amplification is 0.157 ± 0.003 quanta. This is very close to the quantum limit of 0.143 ± 0.006 quanta for our power gain G, as given by Eq. (1). The bandwidth and saturation power of the amplification is 4 MHz and −131 dBm, respectively.

Results and discussion

Theoretical model and experiment

The theoretical model is illustrated in Fig. 1a, b. We consider a superconducting artificial atom, an M-level transmon[24], at the end of a semi-infinite transmission line[16,22]. A strong resonant pump field is fed into the atom from the open end, exciting the transmon from its ground state $|0\rangle$ to a particular excited state $|N\rangle$ by absorbing N photons. In order to probe the transmon dressed by the pump, we apply a weak probe field, whose Rabi frequency Ω_p is much smaller than the transmon decoherence rate γ_{10}, and analyze the power reflectance $|r|^2$ of this probe. The results show that amplification ($|r|^2 > 1$) is caused by the probe photons being resonant with the dressed states exhibiting population inversion. Additionally, due to the multiple levels of the transmon, near-resonant transitions from different sidebands constructively contribute to the reflected signal, resulting in an enhancement of the amplification. Conversely, attenuation ($|r|^2 < 1$) occurs when the population between dressed states is not inverted. The theoretical description of the system's dynamics and the calculation of reflectance are discussed in the "Methods" section.

We characterize the basic properties of the artificial atom through single-tone scattering[14,20]. We employ two-tone, three-tone, and four-tone spectroscopies to characterize the energy structure of the transmon (see Supplementary Information Note 2 for details). All the extracted parameters are summarized in Table 1. Note that we, throughout the manuscript, calibrate the incident field by measuring the reflected field when the qubit is far detuned. In the measurements of amplification, we focus on the case of three-photon pumping, in which we observe quantum coherence between Rabi sidebands. We also investigate the two- and four-photon pumping cases in Supplementary Information Notes 3 and 5, respectively. The maximum power amplification obtained for all three pumping cases is given in Supplementary Information Table 2.

In the three-photon-pumping experiment, we pump the $|0\rangle \rightarrow |3\rangle$ transition of the transmon with the experimental setup in Fig. 1c. When this pump is resonant, the frequencies of three pump photons sum up to $\omega_{30} = \omega_{10} + \omega_{21} + \omega_{32}$. Therefore, we set the pump frequency to $\omega_{\text{pump}}/2\pi = \omega_{30}/6\pi = 4.530$ GHz, indicated by the purple arrow in Fig. 2a, b, and sweep the pump power P_{pump} from −125 to −85 dBm. To probe the driven system, we simultaneously sweep a weak continuous probe field at frequency ω_p over a wide range of frequencies, including higher transitions. The experimental data for the reflectance $|r|^2$ of the probe field are shown in Fig. 2a and the corresponding numerical simulation is shown in Fig. 2b.

In Fig. 2a, the dashed curves show the numerically calculated Rabi sidebands resulting from transitions between dressed states in Fig. 1b (see Supplementary Information Note 6 for details). Note that the number of Rabi sidebands is predicted to be $N(N+1)$ in ref. 23. Taking $N = 3$ as in ref. 23 would yield 12 sidebands, which is inconsistent with the measured results (14 sidebands). This disagreement is due to the effect of higher transmon levels than those considered in ref. 23, which become important here due to our strong pumping leading to three-photon processes. The strong pumping in our experiments leads to the emergence of additional transitions, some of which lie outside the measured frequency range. For $P_{\text{pump}} > -95$ dBm, transitions involving dressed states, $|D_i, F+1\rangle \leftrightarrow |D_j, F\rangle$, where $i > j$ ($i < j$), lead to amplification (attenuation) when $\omega_p > \omega_{\text{pump}}$ ($\omega_p < \omega_{\text{pump}}$). This observation can be explained by the population distribution of the dressed states in Supplementary Information Fig. 9. Amplification (attenuation) occurs when population inversion (non-inversion) takes place among the dressed states.

At low pump powers, when $P_{\text{pump}} \sim -120$ dBm, only a single response is visible in the reflectance spectrum in Fig. 2a, b, around the $|0\rangle \leftrightarrow |1\rangle$ transition frequency, in the form of split bright stripes. As the pump power increases, we observe a clear and increasing splitting around the resonance frequency $\omega_{10}/2\pi = 4.766$ GHz. This effect is detuned Autler–Townes splitting[25] (detuning $\Delta = \omega_{\text{pump}} - \omega_{21} = -2\pi \times 8$ MHz), suggesting that there are dressed states formed by the bare states $|1\rangle$ and $|2\rangle$ with the pumping field. Details are shown in Supplementary Information Fig. 12. When the pump power increases further, beyond −110 dBm, we observe multiple Rabi sidebands, which correspond to various transitions between the dressed states. The Rabi sidebands appear as amplification or attenuation of the weak probe field.

The maximum amplification occurs when the signals of the two amplified Rabi sidebands $|D_3, F\rangle \leftrightarrow |D_4, F+1\rangle$ [label (i)] and $|D_4, F\rangle \leftrightarrow |D_5, F+1\rangle$ [label (ii)] in Fig. 2b cross at frequency $\omega_p/2\pi \approx 4.739$ GHz and pump power −95 dBm, interfering constructively. As the near-resonant transitions involving two different transition paths can take place at the same time, an emitted photon from one path triggers the emission of both transitions, thus contributing to the amplification in a collective way. The degree of enhancement can be calculated more accurately by explicitly considering multiple sideband cross-coherences, as shown in ref. 26.

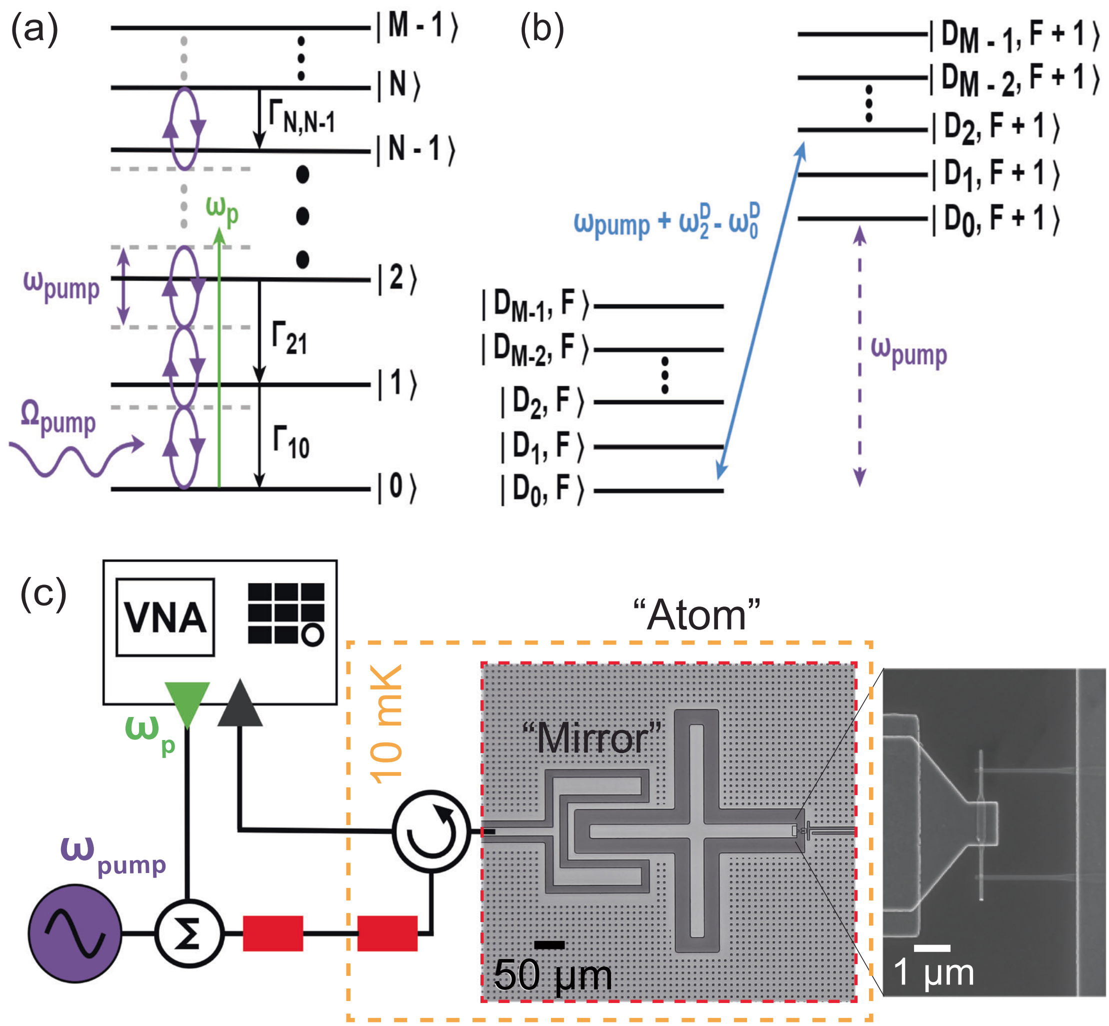

Fig. 1 | The pump-probe scheme and the experimental setup. a An M-level transmon is pumped by a strong resonant field with Rabi (carrier) frequency $\Omega_{\rm pump}$ ($\omega_{\rm pump}$). The Rabi frequency is related to the radio-frequency (RF) power through $\Omega = k\sqrt{P}$, where k is a coupling constant and P is the RF power[14]. The transmon is pumped from $|0\rangle$ to $|N\rangle$ by an N-photon absorption process. A weak probe with frequency $\omega_{\rm p}$ is applied to the system. The relaxation rate between adjacent states $|N\rangle$ and $|N-1\rangle$ is denoted by $\Gamma_{N,N-1}$. **b** Energy diagram of the dressed states in the rotating frame of a pump frequency $\omega_{\rm pump}$. Here D_i ($i = 0, 1, \ldots, M-1$) is the ith eigenstate (with energy $\hbar\omega_i^{\rm D}$) of the system with Hamiltonian $H'_{\rm a} = H_{\rm a} + H_{\rm d}$ ($H_{\rm a}$ and $H_{\rm d}$ are defined in Eqs. (4) and (5), respectively, in the "Methods" section) and F denotes the photon number. The dashed purple line represents the pump frequency $\omega_{\rm pump}$ and the solid blue double-sided arrow indicates the transition between dressed states (see Supplementary Information Note 6 for more details). **c** A simplified circuit diagram of the experimental setup where a probe field (green) and a pump field (purple) are combined by an RF combiner at room temperature with attenuation (red rectangle) and fed into the sample (optical micrograph inside the red dashed box). The micrograph shows an artificial atom (transmon), formed by a large cross-shaped island, capacitively coupled to the end of a semi-infinite transmission line, with a characteristic impedance of $Z_0 \simeq 50\ \Omega$. The reflected output field is measured in a vector network analyzer (VNA). The position of the superconducting quantum interference device (SQUID) loop of the transmon is shown in the scanning electron micrograph on the right. The yellow dashed box shows the cryogenic environment of the dilution refrigerator. Further details on the experimental setup are given in Supplementary Information Note 1.

Table 1 | Extracted and derived transmon parameters

E_C/h [MHz]	E_J/h [GHz]	E_J/E_C –	$\omega_{10}/2\pi$ [GHz]	$\omega_{21}/2\pi$ [GHz]	$\omega_{32}/2\pi$ [GHz]	$\omega_{43}/2\pi$ [GHz]	$\Gamma_{10}/2\pi$ [MHz]	$\Gamma_1^\phi/2\pi$ [MHz]	$\gamma_{10}/2\pi$ [MHz]
228	13.67	59.96	4.766	4.538	4.287	4.005	2.264	0.0317	1.164

We extract the transition frequency ω_{10}, the relaxation rate Γ_{10}, and the decoherence rate γ_{10} by fitting the magnitude and phase data from single-tone scattering (see Supplementary Information Fig. 2b)[34]. We calculate the pure dephasing rate Γ_1^ϕ from Γ_{10} and γ_{10}, using $\gamma_{10} = \Gamma_{10}/2 + \Gamma_1^\phi$. From the four-tone spectroscopy (see Supplementary Information Fig. 2d), we extract ω_{21}, ω_{32}, and ω_{43}, and the anharmonicity between the $|0\rangle \leftrightarrow |1\rangle$ transition and the $|1\rangle \leftrightarrow |2\rangle$ transition. The anharmonicity approximately equals the charging energy[24] E_C. We calculate the Josephson energy E_J and E_J/E_C from ω_{10} and E_C, where $\hbar\omega_{10} \simeq \sqrt{8E_JE_C} - E_C$.

Figure 2c shows the experimental measurement (dots) and numerical simulation (black solid curve) of a horizontal linecut at maximum amplification (indicated by red arrows in Fig. 2a, b). A zoomed-in view of the amplified Rabi sidebands crossing, where we observe quantum coherence, is provided in Supplementary Information Note 4. The solid blue curve represents the theoretical curve without quantum coherence between the amplified Rabi sidebands[26]. The amplified peak has a full width at half maximum (FWHM) of 4 MHz, revealing a maximum power amplification of 1.402 ± 0.025. The data and the simulations are in excellent agreement without any free-fitting parameters.

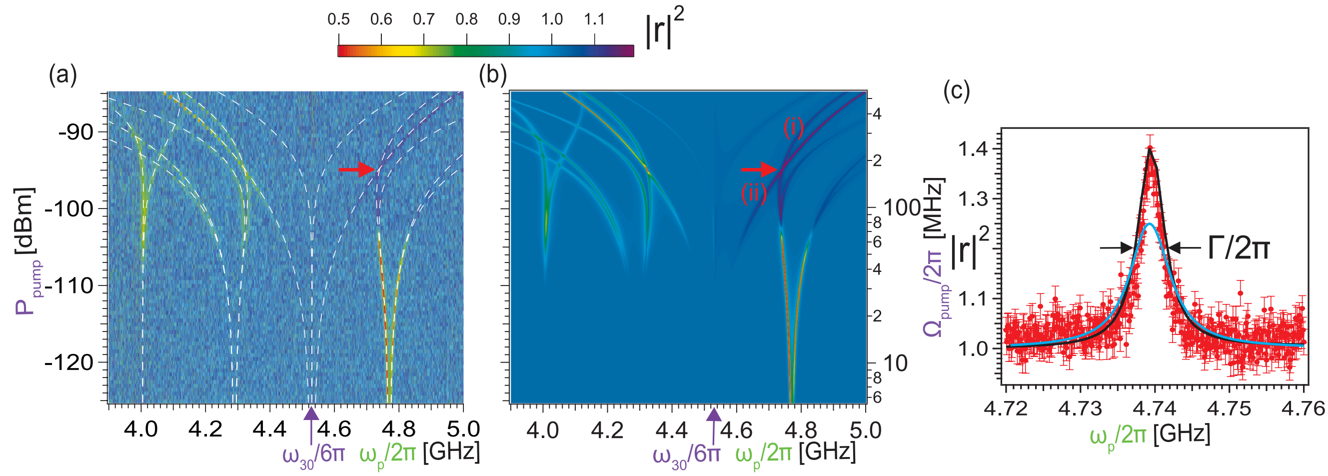

Fig. 2 | Reflectance of a weak probe with three-photon pumping. **a** Measured reflectance spectra $|r|^2$ of the weak probe field ($P_{\mathrm{p}} = -161$ dBm) as a function of probe frequency ω_{p} (x-axis) and pump power P_{pump} (y-axis). The pump frequency is $\omega_{\mathrm{pump}} = \omega_{30}/3 = 2\pi \times 4.530$ GHz. **b** Numerical simulation of the experiment. The left y-axis is the pump power; the right y-axis is the Rabi frequency Ω_{pump}. We set $M = 6$ and use the relaxation rates $\Gamma_{n,n-1}/2\pi = n\Gamma_{10}/2\pi = 2.264n$ MHz, where $n = 1, 2, \ldots, 5$. There are no free fitting parameters for the simulation. **c** A linecut taken at $P_{\mathrm{pump}} = -95$ dBm from Supplementary Information Fig. 4, where the two amplified Rabi sidebands cross each other at $\omega_{\mathrm{p}}/2\pi \approx 4.739$ GHz (indicated by a red arrow in Fig. 2a, b), shows a maximum reflectance 1.402 ± 0.025. The black arrows indicate the width of the reflectance spectrum ($\Gamma/2\pi \sim 4$ MHz). The solid red dots are the experimental data with standard deviation, the solid black curve is the linecut of the numerical simulation from **b**, and the solid blue curve is the theoretical result without quantum coherence between the amplified Rabi sidebands[26]. The excess gain (black) is about twice that of the case without quantum interference (blue). The roughly 2% difference between data and theory from 4.72 to 4.73 GHz is most likely due to the gain drift of the HEMT amplifier (see Supplementary Information Fig. 1) measured with the background (reference) reflectance.

It is important to further examine the amplification properties of the system. Figure 3a shows the measured saturation of the amplification process as a function of probe power P_{p} (Rabi frequency Ω_{p}) at the maximum amplification point. The details of the measurements, including more data, are provided in Supplementary Information Note 7. We observe a maximum power amplification of 1.405 ± 0.072 in the regime of weak probe power. As we increase P_{p} (Ω_{p}) beyond the saturation power P_{sat}, the amplification begins to saturate towards unity. We also studied gain limitations; see Supplementary Information Note 4A for more details. Approximately half of the excess maximum reflectance is $|r|^2 \simeq 1.2$. The probe power and Rabi frequency at this reflectance correspond to the saturation power P_{sat} and linewidth $\Gamma/2\pi$, respectively, as indicated by the markers. The saturation power P_{sat} is related to the linewidth of the dressed state by $P_{\mathrm{sat}} = \hbar\omega_c\Gamma \simeq -131$ dBm, where ω_{c} and Γ are the resonance frequency and the linewidth of the dressed state, respectively.

To further understand the noise properties at the point of maximum amplification, we drove the transmon at a resonant three-photon pump frequency. We then measured the inelastic (incoherent) spectrum of spontaneous emission at frequencies near the maximum amplification point using the experimental setup shown in Supplementary Information Fig. 1b, with a resolution bandwidth of 910 kHz. We also measured this spectrum with the pump turned off. The power spectral density (PSD), normalized to a single photon energy quantum, shown in red on the left y-axis in Fig. 3b, is obtained by subtracting the pump-off from the pump-on spectral curve and calibrating the absolute power (see Supplementary Information Note 8). The inelastic (incoherent) spectrum reveals a peak due to the finite population of excited states among the dressed states.

The PSD quantifies the intensity of the noise at the frequency of the maximum amplification point produced by the spontaneous emission. Since PSD can be directly converted to a noise temperature T_{N}, we determined the noise temperature of the amplification from this data. The resulting curve (blue, right y-axis) in Fig. 3b corresponds to the horizontal linecut from Supplementary Information Fig. 11a, b at $P_{\mathrm{pump}} = -96.5$ dBm (see Supplementary Information Note 8 for details) and shows good agreement with the numerical simulation. We summarize the peaks of gain, noise, and quantum-limited noise in the cases without and with interference in Table 2, suggesting that nearly quantum-limited microwave amplification

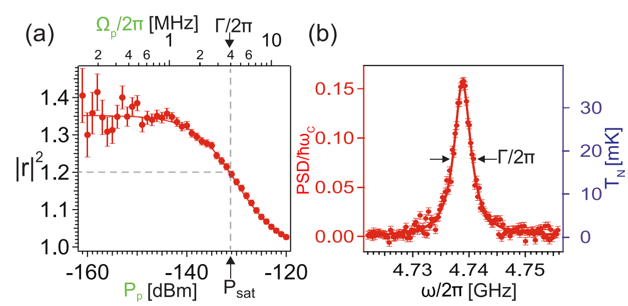

Fig. 3 | Saturation and noise properties of the amplification process (Figures 2a and 3 were measured in different cooldowns with the same sample). Solid dots represent experimental data with standard deviation; solid red curves show the results of numerical simulations. We set the pump frequency to a fixed value of $\omega_{30}/6\pi = 4.530$ GHz, and the pump power to $P_{\mathrm{pump}} = -96.5$ dBm. **a** Measured reflectance $|r|^2$ as a function of probe power P_{p} (bottom x-axis) at the point where we observed the maximum power amplification (1.405 ± 0.072) at weak probe power. The top x-axis shows the Rabi frequency Ω_{p}. **b** At the maximum amplification point, the pump field induces a population inversion between the states $|D_3, F\rangle \leftrightarrow |D_4, F+1\rangle$ [label (i)] and $|D_4, F\rangle \leftrightarrow |D_5, F+1\rangle$ [label (ii)]. This population inversion leads to the spontaneous emission of photons, as depicted in the measured spectrum in red on the left y-axis as a function of frequency ω. The spectrum reveals the characteristic emission profile corresponding to these states. The noise temperature, crucial for amplifier operation, is shown in blue on the right y-axis. The arrows indicate the width of the spectrum ($\Gamma/2\pi \sim 4$ MHz).

Table 2 | The peak values of power gain, noise, and quantum-limited noise (expressed in units of quanta), with and without interference effects between Rabi sidebands in the stimulated emission

	Without interference	With interference
Gain	1.25	1.402 ± 0.025
Noise	0.157	0.157 ± 0.003
Quantum-limited noise	0.10	0.143 ± 0.006

The quantum-limited noise increases as the gain increases, according to Eq. (1).

is achieved by interfering with degenerate stimulated emission in a single artificial atom.

The observed linewidth $\Gamma/2\pi$ in Figs. 2c and 3b is due to the minimal effect of pure dephasing ($2\gamma \simeq \Gamma$, where γ is the decoherence rate and Γ is the linewidth of the dressed state at the crossing point). Figure 2c shows the measurements conducted using a vector network analyzer (VNA) employing two fields (pump and probe), which primarily explore elastic (coherent) scattering of the probe, aiming at measuring stimulated emission among dressed states. In contrast, Fig. 3b shows the measurement of spontaneous emission with a spectrum analyzer (SA) utilizing a single RF source as a pump field. This configuration captures the spontaneous emission of the atom, directly related to inelastic (incoherent) scattering[6]. The use of both instruments enabled the exploration of different quantum processes occurring among the dressed states.

In conclusion, we investigated the amplification of a weak probe field by a single artificial atom at the end of a semi-infinite transmission line due to multi-photon excitations in dressed states induced by a strong pump field. The reflectance of the weak probe displayed multiple Rabi sidebands, which were either amplified or attenuated. We observed a particularly strong amplification when two amplified Rabi sidebands crossed, leading to constructive interference between the emitted photons. In one such case, we observed a power amplification of 1.402 ± 0.025. About half of the excess gain there can be attributed to quantum interference. We found, by analyzing the spectrum of spontaneous emission, that the added noise of the amplification process was nearly quantum-limited at 0.157 ± 0.003 quanta; the quantum limit was 0.143 ± 0.006 quanta for this level of amplification. We thus demonstrated that nearly quantum-limited microwave amplification can be achieved by interferingwith degenerate stimulated emission in a single artificial atom.

Methods

System dynamics and calculation of reflectance

The dynamics of an artificial atom at the end of a semi-infinite transmission line under a multi-photon drive can be described by the Born–Markov quantum master equation[24,27–29],

$$\frac{d\rho}{dt} = -\frac{i}{\hbar}\left[H_S,\rho\right] + \sum_{n,m=1}^{M-1}\frac{\Gamma_{n,n-1}+\Gamma_{m,m-1}}{2}\mathcal{D}\left[\sigma_{n,n-1},\sigma_{m-1,m}\right]\rho + \Gamma_1^{\phi}\mathcal{D}\left[\sum_{n=1}^{M-1} n\sigma_{n,n},\sum_{m=1}^{M-1} m\sigma_{m,m}\right]\rho, \quad (2)$$

where the system Hamiltonian is given by

$$H_S = H_a + H_d + H_p, \quad (3)$$

with

$$H_a = \sum_{n=1}^{M-1}\hbar\left(\omega_n - n\omega_{\text{pump}}\right)\sigma_{n,n}, \quad (4)$$

$$H_d = \sum_{n=1}^{M-1}\sqrt{n}\frac{\hbar\Omega_{\text{pump}}}{2}\sigma_{n,n-1} + \text{H.c.}, \quad (5)$$

$$H_p = \sum_{n=1}^{M-1}\sqrt{n}\frac{\hbar\Omega_p}{2}\sigma_{n,n-1}e^{-i\left(\omega_p-\omega_{\text{pump}}\right)t} + \text{H.c.} \quad (6)$$

Here, $\sigma_{n,n} = |n\rangle\langle n|$ is the projection operator for the nth energy level with atomic energy $\hbar\omega_n$ and $\sigma_{n,n-1} = |n\rangle\langle n-1|$ is the atomic ladder operator between the nth and $(n-1)$th level of the transmon. The Rabi frequency and the carrier frequency of the pump (probe) field are denoted by Ω_{pump} (Ω_p) and ω_{pump} (ω_p), respectively. The pump frequency ω_{pump} for N-photon pumping is obtained by dividing the relevant transition frequency by N. For instance, in the cases $N = 2$, 3, and 4, the pump frequencies are $\omega_{20}/2$, $\omega_{30}/3$, and $\omega_{40}/4$, respectively. Here, ω_{20}, ω_{30}, and ω_{40} are the transition frequencies for the $|0\rangle \leftrightarrow |2\rangle$, $|0\rangle \leftrightarrow |3\rangle$, and $|0\rangle \leftrightarrow |4\rangle$ transitions, respectively (see Fig. 1a in the main text). The Lindblad superoperator is defined as $\mathcal{D}[A,B]\rho = B\rho A - \frac{1}{2}AB\rho - \frac{1}{2}\rho AB$. The relaxation rate from the level $|n\rangle$ to $|n-1\rangle$ is given by $\Gamma_{n,n-1}$. The last term in Eq. (2) is added to account for the pure dephasing process with the dephasing rate Γ_n^{ϕ} for the nth level. Finally, H.c. stands for Hermitian conjugate.

The reflectance is determined by $|r|^2 = \left|\frac{\langle a_{\text{out}}\rangle}{\langle a_{\text{in}}\rangle}\right|^2$, where the output and input signals are the output annihilation operator a_{out} and the input annihilation operator a_{in}, respectively[30]. The output signal can be determined from the input signal and the atomic response via the input–output relation[31]

$$a_{\text{out}}(t) = a_{\text{in}}(t) - \sum_{n=1}^{M-1}\sqrt{\Gamma_{n,n-1}}\sigma_{n-1,n}(t). \quad (7)$$

In our setup, we apply a single-mode classical probe field as an input signal. Then, the input operator can be approximated by a classical field[32,33]:

$$a_{\text{in}}(t) \rightarrow -\frac{i\Omega_p}{2\sqrt{\Gamma_{10}}}e^{-i\left(\omega_p-\omega_{\text{pump}}\right)t}. \quad (8)$$

Hence, the reflectance due to the weak probe beam is given by

$$|r|^2 = \left|1 - 2i\sum_{n=1}^{M-1}\frac{\sqrt{\Gamma_{10}\Gamma_{n,n-1}}\left\langle\sigma_{n-1,n}(t)\right\rangle}{\Omega_p}\right|^2. \quad (9)$$

Note that we limited the number of energy levels to $M = 6$, considering the population in the state $|5\rangle$ to be negligible. In numerical calculations, we thus considered the sum of five atomic transitions $\left\langle\sigma_{n-1,n}\right\rangle$ for $n = 1, 2, \ldots, 5$.

Data availability

The data that supports the findings of this study is available from the corresponding authors upon reasonable request.

Code availability

The code that supports the findings of this study is available from the corresponding authors upon reasonable request.

Received: 17 June 2024; Accepted: 21 February 2025;
Published online: 12 March 2025

References

1. Einstein, A. Zur Quantentheorie der Strahlung. *Phys. Z.* **18**, 121–128 (1917).
2. Liu, J.-M. *Principles of Photonics* (Cambridge University Press, 2016).
3. Caves, C. M. Quantum limits on noise in linear amplifiers. *Phys. Rev. D* **26**, 1817–1839 (1982).
4. Tey, M. K. et al. Strong interaction between light and a single trapped atom without the need for a cavity. *Nat. Phys.* **4**, 924 (2008).
5. Shen, J.-T. & Fan, S. Coherent single photon transport in a one-dimensional waveguide coupled with superconducting quantum bits. *Phys. Rev. Lett.* **95**, 213001 (2005).
6. Astafiev, O. et al. Resonance fluorescence of a single artificial atom. *Science* **327**, 840 (2010).
7. Astafiev, O. V. et al. Ultimate on-chip quantum amplifier. *Phys. Rev. Lett.* **104**, 183603 (2010).
8. Roy, D., Wilson, C. M. & Firstenberg, O. Colloquium: strongly interacting photons in one-dimensional continuum. *Rev. Mod. Phys.* **89**, 021001 (2017).
9. Sheremet, A. S., Petrov, M. I., Iorsh, I. V., Poshakinskiy, A. V. & Poddubny, A. N. Waveguide quantum electrodynamics: collective radiance and photon-photon correlations. *Rev. Mod. Phys.* **95**, 015002 (2023).

10. Hoi, I.-C. et al. Demonstration of a single-photon router in the microwave regime. *Phys. Rev. Lett.* **107**, 073601 (2011).
11. Hoi, I.-C. et al. Generation of nonclassical microwave states using an artificial atom in 1D open space. *Phys. Rev. Lett.* **108**, 263601 (2012).
12. Hoi, I.-C. et al. Giant cross-Kerr effect for propagating microwaves induced by an artificial atom. *Phys. Rev. Lett.* **111**, 053601 (2013).
13. van Loo, A. F. et al. Photon-mediated interactions between distant artificial atoms. *Science* **342**, 1494 (2013).
14. Hoi, I.-C. et al. Probing the quantum vacuum with an artificial atom in front of a mirror. *Nat. Phys.* **11**, 1045 (2015).
15. Forn-Díaz, P. et al. Ultrastrong coupling of a single artificial atom to an electromagnetic continuum in the nonperturbative regime. *Nat. Phys.* **13**, 39 (2017).
16. Wen, P. Y. et al. Large collective Lamb shift of two distant superconducting artificial atoms. *Phys. Rev. Lett.* **123**, 233602 (2019).
17. Mirhosseini, M. et al. Cavity quantum electrodynamics with atom-like mirrors. *Nature* **569**, 692 (2019).
18. Wen, P. Y. et al. Landau–Zener–Stückelberg–Majorana interferometry of a superconducting qubit in front of a mirror. *Phys. Rev. B* **102**, 075448 (2020).
19. Kannan, B. et al. Waveguide quantum electrodynamics with superconducting artificial giant atoms. *Nature* **583**, 775 (2020).
20. Lin, W.-J. et al. Deterministic loading of microwaves onto an artificial atom using a time-reversed waveform. *Nano Lett.* **22**, 8137–8142 (2022).
21. Koshino, K. et al. Observation of the three-state dressed states in circuit quantum electrodynamics. *Phys. Rev. Lett.* **110**, 263601 (2013).
22. Wen, P. Y. et al. Reflective amplification without population inversion from a strongly driven superconducting qubit. *Phys. Rev. Lett.* **120**, 063603 (2018).
23. Wiegand, E., Wen, P.-Y., Delsing, P., Hoi, I.-C. & Kockum, A. F. Ultimate quantum limit for amplification: a single atom in front of a mirror. *N. J. Phys.* **23**, 043048 (2021).
24. Koch, J. et al. Charge-insensitive qubit design derived from the Cooper pair box. *Phys. Rev. A* **76**, 042319 (2007).
25. Autler, S. H. & Townes, C. H. Stark effect in rapidly varying fields. *Phys. Rev.* **100**, 703–722 (1955).
26. Lin, K.-T., Hsu, T., Lin, Y.-C., Hoi, I.-C. & Lin, G.-D. Signal amplification assisted by multiple sideband interference in 1D waveguide QED systems. arXiv:2307.11174 (2023).
27. Lin, K.-T., Hsu, T., Lee, C.-Y., Hoi, I.-C. & Lin, G.-D. Scalable collective lamb shift of a 1d superconducting qubit array in front of a mirror. *Sci. Rep.* **9**, 19175 (2019).
28. Carmichael, H. J. *Statistical Methods in Quantum Optics 1: Master Equations and Fokker–Planck Equations* (Springer Science & Business Media, 2013).
29. Bishop, L. S. *Circuit Quantum Electrodynamics* (Yale University, 2010).
30. Gardiner, C. W. & Collett, M. J. Input and output in damped quantum systems: quantum stochastic differential equations and the master equation. *Phys. Rev. A* **31**, 3761–3774 (1985).
31. Lalumière, K. et al. Input–output theory for waveguide QED with an ensemble of inhomogeneous atoms. *Phys. Rev. A* **88**, 043806 (2013).
32. Strandberg, I., Lu, Y., Quijandría, F. & Johansson, G. Numerical study of Wigner negativity in one-dimensional steady-state resonance fluorescence. *Phys. Rev. A* **100**, 063808 (2019).
33. Lu, Y. et al. Propagating Wigner-negative states generated from the steady-state emission of a superconducting qubit. *Phys. Rev. Lett.* **126**, 253602 (2021).
34. Lu, Y. et al. Characterizing decoherence rates of a superconducting qubit by direct microwave scattering. *npj Quantum Inf.* **7**, 35 (2021).

Acknowledgements

I.-C.H. acknowledges financial support from the City University of Hong Kong through the start-up project 9610569, from the Research Grants Council of Hong Kong (Grant number 11312322), and from the Guangdong Provincial Quantum Science Strategic Initiative (Grant Nos. GDZX2203001, GDZX2303005, and GDZX2403001). K.-T.L. and G.D.L. acknowledge support from NSTC of Taiwan under projects 112-2112-M-002 -001, 112-2811-M-002-067, 113-2112-M-002-025, and NTU under project NTU-CC-110L890106. A.F.K. acknowledges support from the Swedish Research Council (grant number 2019-03696), the Swedish Foundation for Strategic Research, the Horizon Europe program HORIZON-CL4-2022-QUANTUM-01-SGA via the project 101113946 OpenSuperQPlus100, and from the Knut and Alice Wallenberg Foundation through the Wallenberg Centre for Quantum Technology (WACQT). J.C.C. acknowledges financial support from the NSTC of Taiwan under projects 110-2112-M-007-022-MY3 and 111-2119-M-007-008. H.I. acknowledges support from FDCT Macau under grants 0130/2019/A3 and 0015/2021/AGJ and support from the University of Macau under grant MYRG2018-00088-IAPME. P.Y.W. acknowledges financial support from the NSTC of Taiwan under project 110-2112-M-194-006-MY3.

Author contributions

I.-C.H. conceived and organized the project. F.A. and P.-Y.W. performed the experiments and analyzed the results with assistance from Samina, C.-P.L., Y.-T.C., C.-Y.C., C.-H.C., K.-M.H., and Y.-H.H. K.-T.L. developed the theory model and performed the theoretical simulation of the experiments with the help of Y.-C. and E.W. Y. L., H.-T.H., H.I., J.-C.C., and Y.-H.L. engaged in discussions. A.F.K. and G.-D.L. provided theory support. F.A., K.-T.L., and P.-Y.W. contributed to the writing of the manuscript with input from all other authors. A.F.K. and I.-C.H. edited the manuscript. All authors reviewed the manuscript. I.-C.H. supervised the project.

Competing interests

The authors declare no competing interests.

Additional information

Supplementary information The online version contains supplementary material available at https://doi.org/10.1038/s41534-025-00993-3.

Correspondence and requests for materials should be addressed to Io-Chun Hoi.